Available online at www.sciencedirect.com
ScienceDirect
Journal of Magnetic Resonance 184 (2007) 15–19
JMR Journal of Magnetic Resonance
www.elsevier.com/locate/jmr

Three-dimensional through-bond homonuclear–heteronuclear correlation experiments for quadrupolar nuclei in solid-state NMR applied to ^{27}Al–O–^{31}P–O–^{27}Al networks

Michaël Deschamps *, Dominique Massiot

CRMHT-CNRS, 1D Avenue de la Recherche Scientifique, 45071 ORLEANS cedex 2, France

Received 23 May 2006; revised 12 September 2006
Available online 5 October 2006

Abstract

We present here the first 3D homonuclear/heteronuclear correlation experiment applied to quadrupolar nuclei and making use of the sole scalar *J*-coupling. This experiment, based on the 2D-Homonuclear–Heteronuclear Single Quantum Correlation (H–HSQC) experiment, uses a relayed transfer from the ^{27}Al central transition to neighbouring ^{31}P spins and to the central transition of a second ^{27}Al. It confirms the correlation map characterizing the two ^{27}Al and the ^{31}P NMR signatures of ^{27}Al–O–^{31}P–O–^{27}Al chemically bonded molecular motifs.

Keywords: 3D; *J*-coupling; Quadrupolar nuclei; Aluminium; Phosphate

1. Introduction

3D *J*-mediated correlation experiments have been introduced a long time ago in liquid-state NMR experiments [1]. They enable characterization of triplets of atoms which are connected together, and, as such, are very powerful to characterize the network of chemical bonds in a solution or in a solid-state sample as well. High resolution solid-state experiments can make efficient use of the scalar part of the *J*-coupling in MAS experiments on organic and inorganic solids [2,3], despite the heterogeneous line broadening mechanisms that usually mask the direct spectral expression of the *J*-couplings, taking directly benefits from the increased sensitivity and resolution obtained at high fields and high MAS spinning rates [4]. Aluminophosphates materials ($AlPO_4$) attracted much interest over the last two decades, as a credible alternative to other sorbents and catalysts [5]. Among mesoporous materials made from $AlPO_4$, $AlPO_4$-14 has already been studied by X-ray crystallography [6,7] and NMR [7–9] and will be taken as a demonstration example. Its structure is well known and similar to those of zeolithes, but the framework is entirely built up with AlO_x and PO_4 polyhedrons. Four, five and sixfold coordination states are observed for the Al atoms and Al are connected together by either bridging oxygen atoms or O–P–O chains. Four different sites can be distinguished for Al and also for P atoms [7]. Al_1 is fivefold coordinated trigonal–bipyramidal (bonded to 4 –O–P–$(O–Al)_4$ and 1 –O–Al), Al_2 and Al_3 are fourfold coordinated tetrahedra (bonded to 4 –O–P–$(O–Al)_4$) and Al_4 is a sixfold coordinated octahedra (bonded to 4 –O–P–$(O–Al)_4$ and 2 –O–Al).

In contrast with liquid-state experiments in which short relaxation times of quadrupolar nuclei often precludes the proper manipulation of quadrupolar spins, several 2D dipolar mediated or *J*-mediated homonuclear and heteronuclear correlation methods have been introduced for

* Corresponding author. Fax: +33 2 38 63 81 03.
E-mail address: michael.deschamps@cnrs-orleans.fr (M. Deschamps).

1090-7807/$ - see front matter © 2006 Elsevier Inc. All rights reserved.
doi:10.1016/j.jmr.2006.09.011

solid-state experiments involving one or two quadrupolar nuclei like ^{27}Al ($S = 5/2$) [7,9–13], ^{71}Ga ($S = 3/2$) [14] or ^{27}Al and ^{17}O ($S = 5/2$) [15]. The efficiency of ^{27}Al/ ^{31}P ($S = 1/2$) experiments benefits from their 100% natural abundance and their good receptivity, with increased sensitivity at high field by diminishing the second order quadrupolar broadening of ^{27}Al dimensions [16]. Moreover, the magnetization of the ^{27}Al central transition (which is only affected by the second-order quadrupolar broadening) can be efficiently enhanced by populating the central transition from the outer satellites using methods like DFS or RAPT [17,18]. In this contribution we show that it is possible, in solid-state, to characterize structural motifs involving three different spins (2 ^{27}Al and 1 ^{31}P in a Al–O–P–O–Al linkage) in a three-dimensional experiment that correlates the 1D spectra of the three bonded cation nuclei ($2\times{}^{27}$Al and $1\times{}^{31}$P). Because we use the scalar coupling J_2(X–O–Y), the 3D H–HSQC spectrum allows an identification of molecular entities extending over 4 chemical bonds and typically over 0.4 to 0.5 nm in size. Despite its low sensitivity, this experiment provides a new and unique way for obtaining unambiguously this type of information.

2. Results and discussion

The new 3D homonuclear/heteronuclear correlation experiment (3D H–HSQC) that we developed makes use of the sole scalar J-coupling to transfer the magnetization. This results in a robust and rather simple pulse sequence that only involves manipulation of the spin system with soft $\pi/2$ and π pulses, which ensures manipulation of the ^{27}Al central transition as a fictitious spin 1/2. The transfer occurs from the first aluminium atom to the neighbouring phosphorus and then to a second aluminium through the isotropic scalar part J_2(Al–O–P) of the J-coupling in an Al–O–P–O–Al group. This pulse sequence is the extension of the 2D-Homonuclear–Heteronuclear Single Quantum Correlation (H–HSQC) experiment that we recently described [13], obtained by introducing an additional evolution time t_2 encoding the ^{31}P isotropic dimension (Fig. 1). It provides experimental evidence for through-bond correlations between X_1, Y and X_2 nuclei in X_1–O–Y–O-X_2 motives with spectral identification of the resonances of these three nuclei in the different projections. Because the experiment uses the scalar coupling it does not require any reintroduction of interaction averaged out by MAS and it undergoes no limitation with the spinning rate which is usually required to achieve better resolution. It only requires long enough transverse relaxation times T_2' (typically 15 ms in our case) and a sufficient sensitivity for the acquisition of the 3D dataset within a reasonable experimental time.

The experiment consists in two INEPT transfers separated by a constant time period achieving the magnetization transfer and containing the ^{31}P encoding time t_2. The first INEPT transfer leads to the creation of a density operator proportional to $2\mathrm{Al}^1_{z,\mathrm{CT}}\mathrm{P}_y$ (where the aluminium

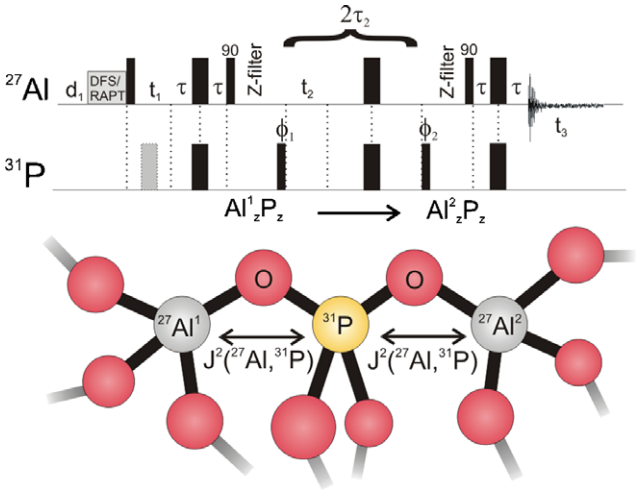

Fig. 1. Pulse sequence for the 3D (t_1 and t_2 incremented) H–HSQC experiment. A scheme of the atoms and the scalar couplings involved is shown below in the ^{27}Al/^{31}P case. The $2\tau_2$ delay is a constant time period allowing for the magnetization transfer from the Al_1 spin to the Al_2 spin. $^{27}\mathrm{Al}_1$ and ^{31}P chemical shift evolutions occur during the t_1 and t_2 delays respectively. Two Z-filters (300 rotor periods or 21 ms) have been used to suppress unwanted contributions. τ and τ_2 were set to 40 rotor periods (2.86 ms) and 120 rotor periods (8.57 ms), respectively, with a MAS speed of 14 kHz and $B_0 = 17.63$ T (750 MHz ^{1}H Larmor frequency). $\Phi_1 = \{0°, 180°\}$, $\Phi_2 = \{0°, 0°, 180°, 180°\}$ and $\Phi_{\mathrm{rec}} = \{0°, 180°, 180°, 0°\}$.

central transition is described as a fictitious spin 1/2) after an evolution under the scalar coupling during a delay 2τ ($1/4J$). The second constant time echo period ($2\ \tau_2$) allows for the conversion of $\mathrm{Al}^1_{z,\mathrm{CT}}\mathrm{P}_y$ into $\mathrm{Al}^2_{z,\mathrm{CT}}\mathrm{P}_y$, which gives rise to a negative cross-peak in the 2D H–HSQC spectrum. The positive diagonal signal corresponds to the remaining $\mathrm{Al}^1_{z,\mathrm{CT}}\mathrm{P}_y$ term. When each Al atom is bound to four O–P–O–Al groups, the evolution of the density operator during τ_2 is described by [13]:

$$\begin{aligned}\sigma(\tau_2 = 0) &= 2\mathrm{Al}^1_{z,\mathrm{CT}}\mathrm{P}_y \\ \sigma(\tau_2) &= \frac{1}{8}[3 + 4\cos(4\pi J\tau_2) + \cos(8\pi J\tau_2)](2\mathrm{Al}^1_{z,\mathrm{CT}}\mathrm{P}_y)_{diagonal} \\ &\quad + \frac{1}{8}[\cos(8\pi J\tau_2) - 1](2\mathrm{Al}^2_{z,\mathrm{CT}}\mathrm{P}_y)_{\text{cross-peak}}\end{aligned} \tag{1}$$

These equations are plotted in Fig. 2 as a function of τ_2 in $1/J$ units. The ^{31}P chemical shift evolves during the delay t_2, and the ^{31}P scalar couplings to the neighbouring ^{27}Al spins evolve in a constant time manner during $2\tau_2$.

The resulting three-dimensional hypercomplex dataset is Fourier transformed against the three evolution times and Figs. 3B–D shows one ^{27}Al/^{27}Al plane (with the x and y axis corresponding to the direct and indirect ^{27}Al dimensions) extracted from the 3D matrix (as shown in Fig. 3A) and corresponding to the phosphorus chemical shift of the P_2 site $\delta(^{31}\mathrm{P}) = -8.03$ ppm. Hence, this 2D spectrum will feature the negative diagonal peaks of any Al_x–O–P_2 group and the positive cross-peaks of any Al_x–O–P_2–O–Al_y groups. Three different strips along the ^{31}P axis, perpendicular to the ^{27}Al/^{27}Al plane and intersecting

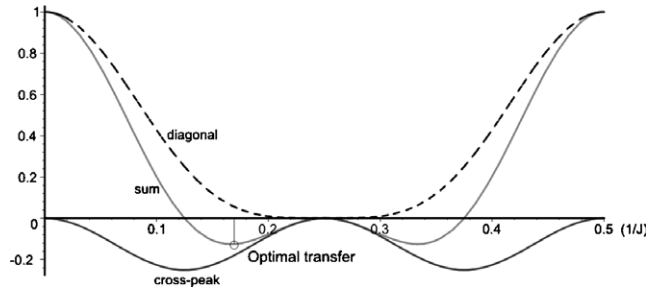

Fig. 2. Plots of the intensities of the diagonal ($2Al^{1}_{z,CT}P_{y}$) and cross-peak ($2Al^{2}_{z,CT}P_{y}$) and their sum (overall signal) as a function of τ_2 in $1/J$ units. The optimum transfer is obtained for the largest negative overall signal (sum of the two contributions).

with it in the cross (indicating an Al_x,Al_y peak), are superimposed on the 2D spectrum. If Al_x and Al_y are also connected via O–P_n–O, the P_n peak will appear in the superimposed strip. In (B), the cross is located on the *negative* (hence diagonal) Al_1, Al_1 peak in the plane corresponding to P_2, indicating that a diagonal peak is observed for the triplet Al_1, P_2, Al_1, and the corresponding strip (intersecting with the Al, Al plane in ($\delta(Al_1)$, $\delta(Al_1)$) as indicated by the cross) along the ^{31}P axis features three additional peaks corresponding to P_1, P_3 and P_4 indicating that similar Al_1, Al_1 diagonal correlations are observed in the planes corresponding to the chemical shifts of P_1, P_3 and P_4, respectively. Hence, Al_1 is never connected to another Al_1 via an O–P–O group, because only *negative* diagonal peaks have been observed, and Al_1 is bonded to P_1, P_2, P_3 and P_4. In (C), the cross is located on the Al_2, Al_4 cross-peak, indicating that Al_2 and Al_4 are connected via an O–P_2–O linkage (because the extracted 2D spectrum corresponds to P_2). Two peaks are observed in the strip for the chemical shifts of P_2 and P_4, hence the cross-peaks between Al_2 and Al_4 are observed in the two following groups: Al_2–O–P_2–O–Al_4 (observable in the plane $\delta(P_2)$ which is represented in the figure) and Al_2–O–P_4–O–Al_4 (observable in the plane $\delta(P_4)$, not represented here). This complies with the known connectivity table (Table 1) which has been established previously [7,8]. A similar conclusion can be inferred from Fig. 3D, where P_1, P_3 and P_4 connect to both the Al_1 and Al_3 atoms.

3. Conclusions

We have shown that a 3D experiment correlating Al_1, P, Al_2 triplets in Al_1–O–P–O–Al_2 motives is feasible and confirm the connectivity graph of the Al/P network of a com-

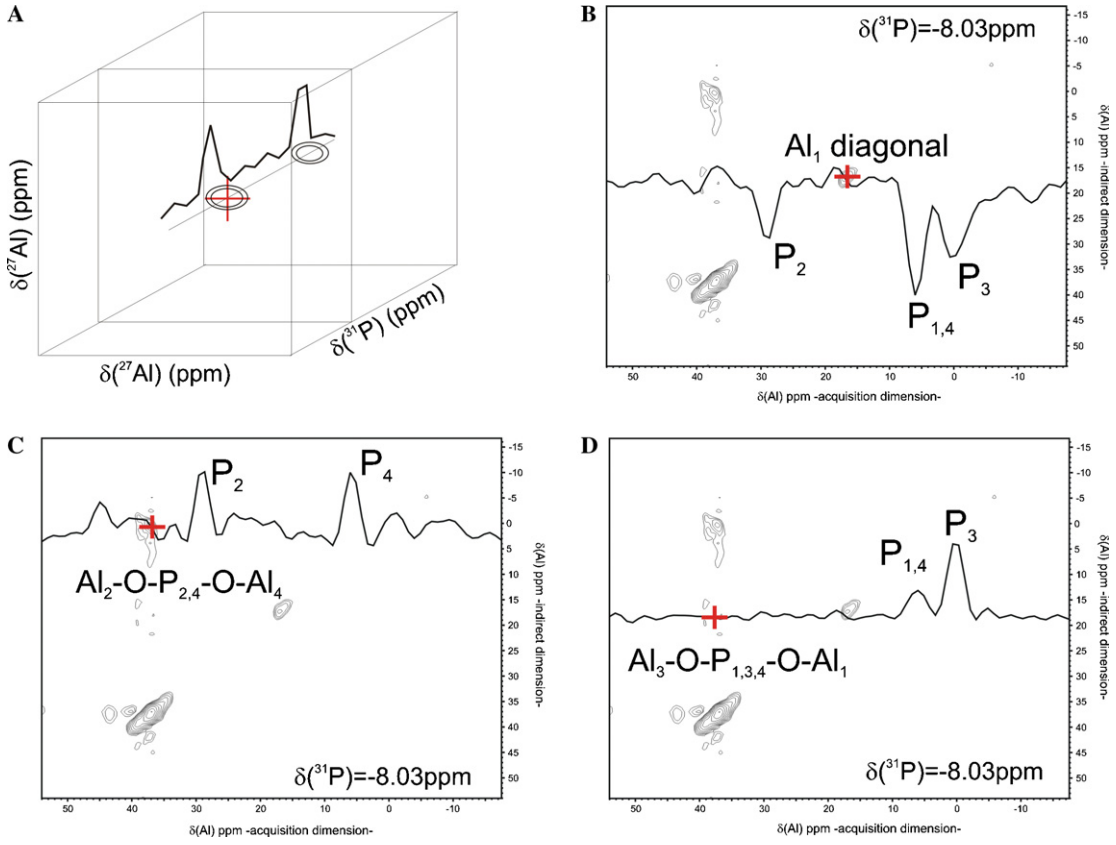

Fig. 3. A 2D plane (as shown in (A)) is extracted from the 3D ^{27}Al,^{31}P,^{27}Al H–HSQC, corresponding to the phosphorus chemical shift $\delta(^{31}P) = -8.03$ ppm (corresponding to P_2) and is displayed three times in (B), (C) and (D). Three different strips or slices along the ^{31}P axis have been extracted, in the manner shown in (A) and are shown in (B), (C) and (D), respectively. In (B), (C) and (D), the respective intersections of the strip with the $^{27}Al/^{27}Al$ plane is indicated by a cross, as shown in the 3D scheme. 1024 scans, 40 increments in F1 and F2, 512 points in F3 and a recycling delay of 250 ms have been used for an overall experimental time of 6 days and 13 h on a 750 MHz wide bore Bruker spectrometer. The data have been processed with nmrPipe [19].

Table 1
Al, P connectivity table for $AlPO_4$-14, as established in Refs. [7,8]

	P_1	P_2	P_3	P_4
Al_1	1	1	1	1
Al_2	2	1	0	1
Al_3	1	0	2	1
Al_4	0	2	1	1

plex material such as $AlPO_4$-14. The significantly longer experimental time required for the 3D experiment (nearly 6 1/2 days), as compared to the 2D Al, Al H–HSQC (1 day), is the price to be paid for the complete edition of connected Al_x–O–P–O–Al_y motives. However, future hardware improvements such as higher magnetic fields, faster MAS rate, the use of magnetic field gradients which will supersede Z-filters (especially in this experiment) and the eventual inclusion of MQMAS and/or ^{1}H decoupling and ^{27}Al satellite transitions refocusing during t_1 might increase the S/N ratio and the available resolution. The principle of this 3D H–HSQC could be extended to any system of three or more coupled spins and applied to many inorganic materials. It provides a detailed map of the coupled network, and a full characterization of chemically bonded molecular motives. When this information remains of little use for crystalline compounds of known structure, recent results show that it becomes decisive information for the characterization of structural motifs at the nanometer scale in amorphous solids or glasses [15].

4. Experimental

Weak (selective, i.e., $\nu_1 \approx 4$ kHz) pulses have been used on the ^{27}Al central transition (described as a fictitious spin 1/2), which is prepared by enhancement from the satellite transitions by DFS [17] transfer using a 2 ms pulse with$\nu_1 \approx 8$ kHz (RAPT [18] can also be used).

Two Z-filters (300 rotor periods or 21 ms) have been used in the pulse sequence to simplify the phase cycle and suppress unwanted contributions of undetermined origin which were observed without the Z-filter. Unfortunately such long Z-filter delays are approaching the order of the T_1 value, and some signal is lost during the Z-filter. A cleaning B_0 field gradient instead would have the desired effect but was unfortunately unavailable on our MAS probes.

The times τ and τ_2 were set to 40 rotor periods (2.86 ms) and 120 rotor periods (8.57 ms), respectively, and the $J^2(^{27}\mathrm{Al},^{31}\mathrm{P})$ values (unobservable in this case) are estimated to be in the 10–30 Hz range. To optimize τ and τ_2, τ_2 was first set to zero and τ has been optimized to get the largest positive signal. Then τ_2 is increased and optimized to obtain the largest negative signal, as shown in Fig. 2. Quantification of the peak intensities requires similar transfer efficiencies: Different T_2 and J-coupling values would lead to different transfer efficiencies, precluding a proper interpretation of the peak intensities.

The MAS speed was set to 14 kHz and a magnetic field $B_0 = 17.63$ T (750 MHz ^{1}H Larmor frequency with ^{27}Al and ^{31}P Larmor frequency equal to 194.47 and 303.67 MHz respectively) was used. 1024 scans, 16 dummy scans, 40 increments in F1 and F2, 512 points in F3 and a recycling delay of 250 ms have been used for an overall experimental time of 6 days and 13 h on a 750 MHz wide bore Bruker spectrometer. The optimum recycling delay, which depends upon the relaxation behaviour of the central and satellite transitions (because DFS is used), was determined by comparing the signal obtained in the permanent regime for various recycling delays, and 250 ms was considered as optimal, as it allowed a 95% recovery.

Indirect quadrature detection was achieved using the States method, whereas DQD was used during acquisition. A spectral width of 14 kHz was used in the three dimensions, corresponding exactly to the MAS spinning speed, in order to sum any remaining spinning sidebands [20]. The data have been processed with nmrPipe [19], the spectrum is phased in order to have negative diagonal peaks and positive cross-peaks, and an exponential line broadening of 200 Hz has been applied in the three dimensions (the natural linewidth in the ^{31}P dimension—without ^{1}H and ^{27}Al decoupling—is about 200 Hz, in the ^{27}Al dimension, second order quadrupolar broadening is larger than the exponential line broadening factor).

Acknowledgments

We acknowledge financial support from CNRS UPR4212, FR2950, MIAT and Région Centre and we are grateful to Pr. P.J. Grandinetti, Drs. F. Fayon and V. Montouillout for stimulating discussions.

References

[1] J. Cavanagh, W.J. Fairbrother, A.G. Palmer, N.J. Skelton Jr., Protein NMR Spectroscopy: Principles and Practice, Academic Press, San Diego, 1996.
[2] D. Sakellariou, L. Emsley, Through-bond experiments in solids, in: D.M. Grant, R.K. Harris (Eds.), The Encyclopedia of NMR, J. Wiley and Sons, London, 2002.
[3] D. Massiot, F. Fayon, B. Alonso, J. Trebosc, J.-P. Amoureux, Chemical bonding differences evidenced from J coupling in solid state NMR experiments involving quadrupolar nuclei, J. Magn. Reson. 164 (2005) 165.
[4] Z. Gan, P. Gor'kov, T.A. Cross, A. Samoson, D. Massiot, Seeking higher resolution and sensitivity for NMR of quadrupolar nuclei at ultrahigh magnetic fields, J. Am. Chem. Soc. 124 (2002) 5634–5635.
[5] T. Wilson, B.M. Lok, C.A. Messina, T.R. Cannan, E.M. Flanigen, Aluminophosphate molecular sieves: a new class of microporous crystalline inorganic solids, J. Am. Chem. Soc. 104 (1982) 1146.
[6] M. Helliwell, V. Kaucic, G.M.T. Cheetham, M.M. Harding, B.M. Kariuki, P.J. Rizkallah, Structure determination from small crystals of two aluminophosphates CrAPO-14 and SAPO-43, Acta Crystallogr. B 49 (1993) 413.
[7] C.A. Fyfe, H. Meyer zu Altenschildesche, K.C. Wong-Moon, H. Grondey, J.M. Chezeau, 1D and 2D solid state NMR investigations of the framework structure of As-synthesized AlPO4-14, Solid State NMR 9 (1997) 97–106.

[8] L. Delevoye, C. Fernandez, C.M. Morais, J.-P. Amoureux, V. Montouillout, J. Rocha, Solid State NMR 22 (2002) 501–512.
[9] J.W. Wiench, M. Pruski, Probing through bond connectivities with MQMAS NMR, Solid State NMR 26 (2004) 51–55.
[10] E.R.H. Van Eck, W.S. Veeman, Solid-state 2D heteronuclear ^{27}Al-^{31}P correlation NMR spectroscopy of aluminophosphate VPI-5, J. Am. Chem. Soc. 115 (1993) 1168–1169.
[11] M. Eden, J. Grinshtein, L. Frydman, High resolution 3D exchange NMR spectroscopy and the mapping of connectivities between half-integer quadrupolar nuclei, J. Am. Chem. Soc. 124 (2002) 9708–9709;
M. Eden, H. Annersten, A. Zazzi, Pulse-assisted homonuclear dipolar recoupling of half-integer quadrupolar spins in magic-angle spinning NMR, Chem. Phys. Lett. 410 (2005) 24–30.
[12] G. Mali, G. Fink, F. Taulelle, Double-quantum homonuclear correlation magic angle sample spinning nuclear magnetic resonance spectroscopy of dipolar-coupled quadrupolar nuclei, J. Chem. Phys. 120 (2004) 2835–2845.
[13] M. Deschamps, F. Fayon, V. Montouillout, D. Massiot, Through-bond homonuclear correlation experiments in solid-state NMR applied to quadrupolar nuclei in Al–O–P–O–Al chains, Chem. Commun. (2006) 1924–1925.
[14] V. Montouillout, C.M. Morais, A. Douy, F. Fayon, D. Massiot, Towards better description of gallo-phosphate materials in solid state NMR: 1D and 2D correlation studies, Magn. Reson. Chem. 8 (2006) 770–775.
[15] D. Iuga, C. Morais, Z. Gan, D.R. Neuville, L. Cormier, D. Massiot, NMR Heteronuclear Correlation between Quadrupolar Nuclei in Solids, J. Am. Chem. Soc. 127 (2005) 11540–11541.
[16] Z. Gan, P. Gor'kov, T.A. Cross, A. Samoson, D. Massiot, Seeking higher resolution and sensitivity for NMR of quadrupolar nuclei at ultrahigh magnetic fields, J. Am. Chem. Soc. 124 (2002) 5634–5635.
[17] A.P.M. Kentgens, R. Verhagen, Advantages of double frequency sweep in static, MAS and MQMAS NMR of spin $I = 3/2$ nuclei, Chem. Phys. Lett. 300 (1999) 435.
[18] H.-T. Kwak, S. Prasad, T. Clark, P.J. Grandinetti, Enhancing sensitivity of quadrupolar nuclei in solid-state NMR with multiple rotor assisted population transfers, Solid State NMR 24 (2003) 71–77.
[19] F. Delaglio, S. Grzesiek, G.W. Vuister, G. Zhu, J. Pfeifer, A. Bax, NMRPipe: a multidimensional spectral processing system based on UNIX pipes, J. Biomol. NMR 6 (1995) 277–293.
[20] D. Massiot, Sensitivity and lineshape improvements of MQ-MAS by rotor synchronized data acquisition, J. Magn. Reson. A 122 (1996) 240–244.